

Structure of two-component Bose-Einstein condensates with respective vortex-antivortex superposition states

Linghua Wen,^{1,2,*} Yongjun Qiao,¹ Yong Xu,^{3,2} and Li Mao²

¹*School of Physical Sciences and Information Engineering, Liaocheng University, Liaocheng 252059, China*

²*Department of Physics, The University of Texas at Dallas, Richardson, Texas 75080, USA*

³*Institute of Physics, Chinese Academy of Sciences, Beijing 100190, China*

(Dated: November 6, 2018)

We investigate the phase structure of two-component Bose-Einstein condensates (BECs) with repulsive intra- and interspecies interactions in the presence of respective vortex-antivortex superposition states (VAVSS). We show that different winding numbers of vortex and antivortex and different intra- and interspecies interaction strengths may lead to different phase configurations, such as fully separated phases, inlaid separated phases, asymmetric separated phase, and partially mixed phases, where the density profile of each component displays a petal-like (or modulated petal-like) structure. A phase diagram is given for the case of equal unit winding numbers of the vortex and antivortex in respective components, and it is shown that conventional criterion for phase separation of two-component BECs is not applicable for the present system due to the VAVSS. In addition, our nonlinear stability analysis indicates that the typical phase structures of two-component BECs with VAVSS allow to be detected in experiments. Moreover, for the case of unequal winding numbers of the vortex and antivortex in respective components, we find that each component in any of the possible phase structures is in a cluster state of vortices and antivortices, where the topological defects appear in the form of singly quantized visible vortex, or hidden vortex, or ghost vortex, depending on the specific parameters of the system. Finally, a general rule between the vortex-antivortex cluster state and the winding numbers of vortex and antivortex is revealed.

PACS numbers: 03.75.Mn, 03.75.Lm, 05.30.Jp, 67.85.Fg

I. INTRODUCTION

Multicomponent systems are of fundamental importance in many fields of physics on account of their universality and complexity. In particular, great attention has been recently paid to a mixture of two-component Bose-Einstein condensates (BECs) in cold atom physics due to ultra high purity, excellent theoretical description, experimental accessibility and precise controllability of a condensate system [1, 2]. Two-component BECs can consist of two different alkalis, or different isotopes, or different hyperfine states of the same alkali atom. Such a mixture provides an attractive and versatile testing ground to study the intriguing properties of macroscopic quantum many-body systems inaccessible in single-component BECs. In fact, many interesting phenomena have been predicted theoretically and some observed experimentally in two-species BECs, ranging from the topological structures of the ground and excited states [3–14], symmetry-breaking transition [15], quantum turbulence [16], pattern formation [17], vortex-bright-solitons [18] and skyrmions [19], entangled states [20], to the stripe phase induced by spin-orbit coupling [21], etc. Among these phenomena, of crucial significance is the phase structure of the system [3–14]. For instance, a separated phase of a two-component BEC is the premise of studying the Kelvin-Helmholtz instability [22] and Rayleigh-

Taylor instability [23].

To the best of our knowledge, most of theoretical literatures use the Thomas-Fermi (TF) approximation (a semi-analytical method) or a variational approach to study the ground state properties of two-component BECs, where spherically symmetric mixed phases, spherically symmetric separated phases, and asymmetric side-by-side separated phases are predicted. For the former case, the kinetic energy is completely neglected. However, when the contribution of kinetic energy to the total energy is considerable, the TF approximation will fail [9] and thus can not be relied upon to determine the phase structure of a two-component BEC. The effect of kinetic energy on the phase transition of a two-component BEC in an infinitely deep square well potential has been recently demonstrated in Ref. [11]. As for the variational approach, it is usually limited to few simple quantum states and certain external potentials. In this context, it is necessary to resort to numerical methods for obtaining reliable phase structures.

In this paper, we investigate the exact two-dimensional (2D) phase structures of two-component BECs with respective vortex-antivortex superposition states (VAVSS). The VAVSS in BECs is a quite interesting research object as it can exhibit rich physical properties [24–28], such as peculiar petal-like structure [24, 25] and unique dynamics [28]. Particularly, the equilibrium properties of a quasi-2D degenerate boson-fermion mixture (DBFM) with a bosonic VAVSS is recently studied by using a quantum-hydrodynamic model [29]. It is shown that the VAVSS greatly influences the equilibrium state and stability of a

*Electronic address: linghuawen@126.com

DBFM, where a special intermittency phenomenon exists in the two stability curves of the DBFM with a bosonic VAVSS [29] and the one with a bosonic vortex [30]. On the other hand, the VAVSS may have many potential applications in quantum information, quantum communication, and inertial sensing [24, 26, 27]. Experimentally, the creation of VAVSS in BECs has been reported by different groups [31–34]. An interesting question is to ask how the phase structure of a two-component BEC is modified by the respective VAVSS combining with intra- and interspecies interactions. We show that, depending on the relative interaction strengths and the winding numbers of vortex and antivortex, the two-component BECs with respective VAVSS can display rich phase structures not met in other systems, such as fully separated phases, in-laid separated phases, and asymmetric separated phase with (deformed) petal-like component density profiles. We give a phase diagram for the case of equal unit winding numbers of vortex and antivortex in respective components. The typical phase structures are long-lived according to our nonlinear stability analysis. For the case of unequal winding numbers of vortex and antivortex, each component in any of the possible phases is in a vortex-antivortex cluster state, where the phase defects emerge in the form of visible vortex, or hidden vortex, or ghost vortex. Furthermore, we reveal and discuss the general relation between the vortex-antivortex cluster state and the winding numbers of vortex and antivortex.

The paper is organized as follows. In Sec. II, we describe the model for two-component BECs with respective VAVSS. In Sec. III, we study the phase structure of two-component BECs with respective VAVSS with equal unit winding numbers of the vortex and antivortex. A phase diagram is presented, and the stability of phase structures is analyzed. In Sec. IV, we discuss the phase structure of the system with unequal winding numbers of the vortex and antivortex in respective components. The conclusion is outlined in the last section.

II. MODEL

We consider a 2D system of trapped two-component BECs with tight confinement in the z direction. In the zero-temperature limit, the dynamics of the system is described by the coupled Gross-Pitaevskii (GP) equations

$$i\frac{\partial\psi_1}{\partial t} = \left[-\nabla_{\perp}^2 + V(r) + g_1|\psi_1|^2 + g|\psi_2|^2\right]\psi_1, \quad (1)$$

$$i\frac{\partial\psi_2}{\partial t} = \left[-\nabla_{\perp}^2 + V(r) + g_2|\psi_2|^2 + g|\psi_1|^2\right]\psi_2, \quad (2)$$

where we have adopted plane-polar coordinates for space (r, θ) , $\nabla_{\perp}^2 = \frac{1}{r}\frac{\partial}{\partial r}(r\frac{\partial}{\partial r}) + \frac{1}{r^2}\frac{\partial^2}{\partial\theta^2}$, and $V(r) = r^2/4$ is the trapping potential. Here we have assumed that the two species have the same atomic mass m and undergo the same trapping frequency ω_{\perp} in the x - y plane. In this paper, length, time, energy, and angular momentum are in units of $d_0 = \sqrt{\hbar/2m\omega_{\perp}}$, $1/\omega_{\perp}$, $\hbar\omega_{\perp}$, and \hbar , respectively.

g_1, g_2 , and g denote dimensionless intra- and intercomponent coupling strengths which are proportional to the corresponding s -wave scattering lengths a_j, a_{ij} ($j = 1, 2$) between intra- and intercomponent atoms and the atom numbers $N_{1,2}$ in species 1 and 2 [1, 2, 28, 29]. The two wave functions are normalized as $\iint |\psi_{1,2}|^2 r dr d\theta = 1$.

We seek dimensionless solutions of stationary VAVSS

$$\psi_j(r, \theta, t) = \varphi_j(r, \theta)e^{-i\mu_j t}, \quad j = 1, 2, \quad (3)$$

where μ_j is the chemical potential, and φ_j is given by

$$\varphi_j(r, \theta) = f_{jk}\alpha_j e^{il_{jk}\theta} + f_{jp}\beta_j e^{i\delta_j} e^{-il_{jp}\theta}, \quad j = 1, 2. \quad (4)$$

Here $f_{jk}(r) = A_j e^{-r^2/2\sigma_j^2} (r/\sigma_j)^{l_{jk}}$ and $f_{jp}(r) = A_j e^{-r^2/2\sigma_j^2} (r/\sigma_j)^{l_{jp}}$ are the amplitudes of the vortex and antivortex components with A_j being the normalization constant and σ_j the width of condensate j . l_{jk} and l_{jp} are the winding numbers of the vortex and antivortex, and the real constants α_j, β_j show the proportion of the vortex and antivortex with $\alpha_j^2 + \beta_j^2 = 1$. The relative phase δ_j just causes offset of the density profile by an angle $\delta_j/(l_{jk} + l_{jp})$. Note that in Eq. (4) we have taken into account the influence of winding number on the condensate size in terms of $\sigma_j^{-l_{jk}}$ and $\sigma_j^{-l_{jp}}$.

Substituting Eq. (3) into Eqs. (1) and (2), we obtain the coupled equations for φ_1 and φ_2 ,

$$\begin{aligned} \mu_1\varphi_1 = & -\frac{1}{r}\frac{\partial}{\partial r}(r\frac{\partial\varphi_1}{\partial r}) + \frac{f_{1p}\beta_1}{r^2}(l_{1p}^2 - l_{1k}^2)e^{i(\delta_1 - l_{1p}\theta)} \\ & + \frac{l_{1k}^2}{r^2}\varphi_1 + (V + g_1|\varphi_1|^2 + g|\varphi_2|^2)\varphi_1, \end{aligned} \quad (5)$$

$$\begin{aligned} \mu_2\varphi_2 = & -\frac{1}{r}\frac{\partial}{\partial r}(r\frac{\partial\varphi_2}{\partial r}) + \frac{f_{2p}\beta_2}{r^2}(l_{2p}^2 - l_{2k}^2)e^{i(\delta_2 - l_{2p}\theta)} \\ & + \frac{l_{2k}^2}{r^2}\varphi_2 + (V + g_2|\varphi_2|^2 + g|\varphi_1|^2)\varphi_2, \end{aligned} \quad (6)$$

where the second and third terms associated with winding numbers in the right-hand sides of Eqs. (5) and (6) are resulted from the presence of VAVSS in each component. Consequently, the chemical potentials $\mu_{1,2}$ read

$$\begin{aligned} \mu_1 = & \frac{2(l_{1k} + 1)}{\sigma_1^2} - \frac{1}{\sigma_1^4} \iint |\varphi_1|^2 r^3 dr d\theta \\ & + \frac{4\pi(l_{1p} - l_{1k})}{\sigma_1^2} \int f_{1p}^2 \beta_1^2 r dr \\ & + \iint [V + g_1|\varphi_1|^2 + g|\varphi_2|^2] |\varphi_1|^2 r dr d\theta, \end{aligned} \quad (7)$$

$$\begin{aligned} \mu_2 = & \frac{2(l_{2k} + 1)}{\sigma_2^2} - \frac{1}{\sigma_2^4} \iint |\varphi_2|^2 r^3 dr d\theta \\ & + \frac{4\pi(l_{2p} - l_{2k})}{\sigma_2^2} \int f_{2p}^2 \beta_2^2 r dr \\ & + \iint [V + g_2|\varphi_2|^2 + g|\varphi_1|^2] |\varphi_2|^2 r dr d\theta, \end{aligned} \quad (8)$$

and they must be determined self-consistently from the normalization conditions of φ_1 and φ_2 .

From Eqs. (5)-(8) we can see that when the kinetic energy is comparable with the sum of interaction energy and potential energy the TF approximation is not suitable to describe the system, especially for cases of VAVSS with large winding numbers. In the following, we numerically solve the coupled equations (5) and (6). Starting with two trial VAVSS with specific ratios of α_j^2 and β_j^2 , we obtain the exact 2D equilibrium state of the system by using the imaginary time propagation method based on the Peaceman-Rachford method [35], which is equivalent to the procedure of minimizing the sum of the average energy per atom in species 1 and that in species 2,

$$E = \iint r dr d\theta [\mu_1 |\varphi_1|^2 + \mu_2 |\varphi_2|^2 - \frac{1}{2} g_1 |\varphi_1|^4 - \frac{1}{2} g_2 |\varphi_2|^4 - g |\varphi_1|^2 |\varphi_2|^2]. \quad (9)$$

III. STRUCTURE OF TWO-COMPONENT BECS WITH RESPECTIVE VAVSS WITH EQUAL WINDING NUMBERS OF VORTEX AND ANTIVORTEX

Here we just consider the case of $\alpha_j^2 = \beta_j^2 = 1/2$ because the petal structure of a VAVSS with unequal superposition ratio only emerges under the condition of a very small particle number or an extremely weak interatomic interaction which is usually not met in experiments [29]. For convenience, we introduce two relative interaction strengths, $R_{21} = g_2/g_1$ and $R = g/g_1$, and assume the intra- and interspecies interactions to be repulsive. Throughout this paper the relative phase is taken to be $\delta_j = 0$. Figure 1 shows the phase diagram of two BECs with VAVSS with $l_{1k} = l_{1p} = 1$ and $l_{2k} = l_{2p} = 1$, where $g_1 = 200$. There exist eight possible phases depending on the values of R_{21} and R , and the typical density profiles corresponding to phases I-VIII are displayed in Fig. 2 and Figs. 3(a)-3(b), respectively. In any of these phases, the density profile of each component displays a petal structure or a crescent-pair (deformed petal) structure or a combined structure of petal and crescent-pair due to the presence of respective VAVSS and the competition between the intraspecies and the interspecies repulsions. In Fig. 1, regions I and IV denote two opposite fully separated phases. In the former phase, component 1 is completely expelled outside component 2 [see Figs. 2(a1) and 2(a2)], while in the latter phase the sequence is converse [Figs. 2(d1) and 2(d2)]. Regions II and III represent two opposite inlaid separated phases, where in the former case species 1 lies separately in the interval between the inner petal layer and the outer crescent layer of species 2, however in the latter case the arrangement of the two species is inverted [Figs. 2(b1)-2(c2)]. Regions V and VI are two different partially mixed phases, where in the first phase species 2 is merged inside species 1 but it is reversed in the second phase [Figs. 2(e1)-2(f2)]. Finally, the vertical solid-line section ($0 \leq R \leq 3.5$) of $R_{21} = 1$ marks a fully mixed phase in which the mixing

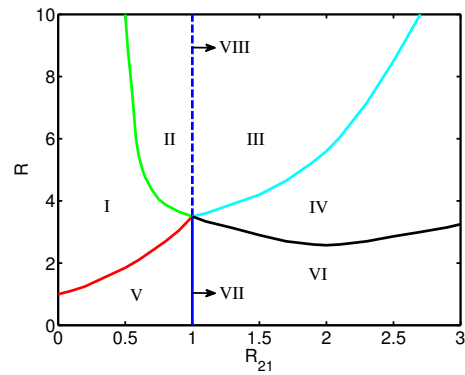


FIG. 1: (color online) Phase diagram of two-component BECs with VAVSS with $l_{jk} = l_{jp} = 1$ ($j = 1, 2$), where $R_{21} = g_2/g_1$ and $R = g/g_1$. The parameters are $g_1 = 200$ and $\alpha_j^2 = \beta_j^2 = 1/2$. Regions I and IV, II and III, and V and VI represent two different fully separated phases, inlaid separated phases, and partially miscible phases, respectively. Vertical solid-line section VII marks a fully mixed phase, while dashed-line section VIII denotes an asymmetric separated phase.

reaches the maximum and the densities profiles of two components are the same [Figs. 3(a1) and 3(a2)], while the vertical dashed-line section ($R > 3.5$) signs an asymmetric separated phase in which both the density profiles are symmetric breaking upon the trap center [Figs. 3(b1) and 3(b2)].

The ground state structure of two-component BECs has been studied by several theoretical [3-8, 10, 11] and experimental groups [13, 14]. A conventional criterion for phase separation is given by $g_1 g_2 < g^2$, which is based on the minimization of the total interaction energy [1, 2]. Note that in the derivation of this criterion the BECs are supposed to be homogeneous and the kinetic energy is neglected. However, the criterion will fail when the kinetic energy becomes important in a nonuniform system. In fact, the kinetic energy play a vital role in determining the configuration of two-component BECs with VAVSS. According to the condition $g_1 g_2 < g^2$, for instance, our system would be in a separated phase if $R_{21} = 2$ and $R > \sqrt{2}$, but only $R > 2.58$ can the actual phase separation occur when $R_{21} = 2$. The similar effect arises for any fixed value of R_{21} or R as shown in Fig. 1. Physically, the kinetic energy acts against the interspecies interaction. The latter is responsible for phase demixing while the former tends to expand the BECs and thus favors phase mixing. At the same time, the trapping potential tends to trap the condensates and hence also sustains phase mixing. Therefore, phase separation can be suppressed by the kinetic energy and external potential in some situations even if the condition $g_1 g_2 < g^2$ is satisfied, as we saw in Figs. 1-3. Recently, the influence of kinetic energy on the mixing-demixing transition by changing the confinement was discussed in Ref. [11]. The authors introduce a parameter $\eta = \int d\vec{r} \psi_1 \psi_2$ to characterize the overlap between two condensate wave functions. And then the system shows phase separation if $\eta \ll 1$. However, nei-

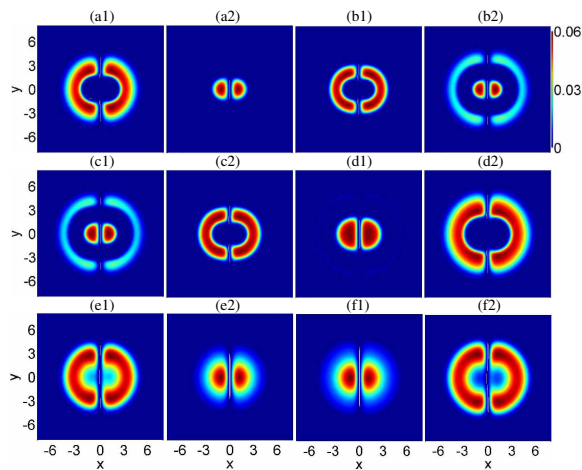


FIG. 2: (color online) Density profiles (a)-(f) correspond to phases I-VI in Fig.1, respectively. Here 1 and 2 label two different components of the system. (a) $R_{21} = 0.2, R = 8$, (b) $R_{21} = 0.8, R = 8$, (c) $R_{21} = 1.5, R = 7$, (d) $R_{21} = 2.5, R = 5$, (e) $R_{21} = 0.6, R = 1$, and (f) $R_{21} = 1.4, R = 1.6$. The other parameters are the same as those in Fig.1. The darker color area indicates the lower density. x and y are in units of d_0 .

ther the criterion $g_1 g_2 < g^2$ nor the condition $\eta \ll 1$ can distinguish different separated phases as shown in Fig. 2 and Fig. 3(b). In addition, from Eqs. (1), (2), (5) and (6), we can see that the two components of the system satisfy the exchange symmetry, which indicates that the phase diagram will be the same if one exchanges the two component wave functions. For fixed values of g_1 and g , nevertheless, two different values of g_2 which are symmetric concerning the line of $R_{21} = 1$ will lead to two different quantum states. The corresponding symmetric one of the interaction set (g_1, g_2, g) is (g_2, g_1, g) [g_1 swaps g_2 , and the set (g_2, g_1, g) is not in the same phase diagram] rather than the set $(g_1, 2g_1 - g_2, g)$ being symmetric about the line of $R_{21} = 1$. This point can explain why the phase diagram in Fig. 1 is asymmetric with respect to the line of $R_{21} = 1$. Here $g_1 = 200$ is a typical parameter value in current experiments. If the value of g_1 does not vary largely, the phase diagram will be basically unchanged except for possible little offset of the boundary lines between different phases. When the value of g_1 changes largely, there exist similar phase structures and the regions corresponding to different phase structures will possibly redistribute in the phase diagram.

The phase structures of two-component BECs with respective VAVSS are obviously different from those of the usual two-component BECs [3–14] by virtue of the petal structure of the VAVSS. On the other hand, the equilibrium properties of the present system are also evidently different from those of DBFM with a bosonic VAVSS [29]. In the latter case, due to the Pauli exclusion principle, there is no s -wave interaction between identical fermions in the spin polarized state. In addition, for the separated phases in the latter case, the gap region between two bosonic petals is always occupied by the Fermi gas,

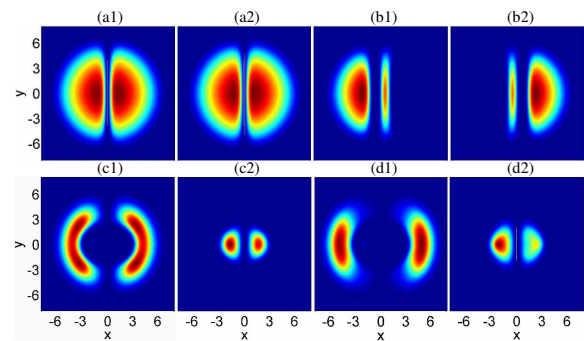


FIG. 3: (color online) (a)-(b): Density profiles (a1)-(a2) and (b1)-(b2) correspond to phases VII and VIII in Fig.1, respectively, where (a) $R_{21} = 1, R = 2$ and (b) $R_{21} = 1, R = 8$. The other parameters are the same as those in Fig.1. (c)-(d): Temporal evolution of density profiles, where the initial state is given by Fig. 2(a) with a random perturbation. The time is (c) $t = 0.4$ and (d) $t = 4$. Here x and y are in units of d_0 , and t is units of $1/\omega_{\perp}$.

while for the fully separated phases and inlaid separated phases in the former case there is no particle occupation in the gap region of two petals of any component due to the interspecies repulsion and the requirement of symmetric petal structure and angular momentum conservation. Furthermore, here the inlaid separated phases and the asymmetric separated phase have no counterparts in DBFM with a bosonic VAVSS.

The VAVSS is a collective excitation (a metastable state) of BECs, which is similar to the case of a single pure vortex state. Although the energy of a VAVSS is higher than that of a pure vortex [25], the configurations of two BECs with VAVSS may be long-lived. To verify this point, we perform a nonlinear stability analysis by monitoring numerically the evolution of a perturbed stationary solution in Eqs.(5) and (6). Shown in Figs. 3(c1)-3(d2) are the time evolution of density profiles, where the initial state is fully separated phase I [see Fig. 2(a)] with a random perturbation. The system will collapse when the initially density profiles begin to deform severely. This method can effectively estimate the lifetime of a VAVSS or a phase structure of the system. As a matter of fact, the nonlinear stability analysis is widely used in the study of solitons [36]. Our simulation shows that the lifetimes of phases I-VII can reach the order of 100 ms and the lifetime of asymmetric separated phase VIII is a bit shorter due to the symmetry breaking, which allows to be detected in experiments. It is deserved to mention that similar phase structures also exist in two-component BECs with VAVSS with higher winding numbers $l_{1k} = l_{1p} = l_{2k} = l_{2p}$. In that case, the stability of phase structures become lower because of the higher energy resulted from the higher winding numbers.

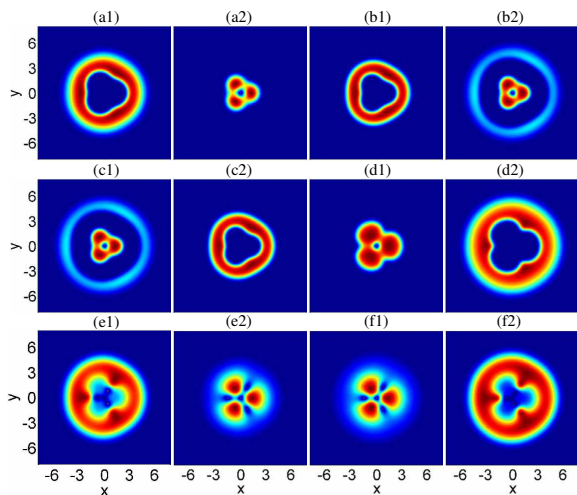


FIG. 4: (color online) Density profiles of two-component BECs with respective VAVSS with $l_{1k} = l_{2k} = 1$ and $l_{1p} = l_{2p} = 2$. (a) $R_{21} = 0.2, R = 8$, (b) $R_{21} = 0.9, R = 8$, (c) $R_{21} = 1.1, R = 7$, (d) $R_{21} = 2.5, R = 5$, (e) $R_{21} = 0.6, R = 1$, and (f) $R_{21} = 1.4, R = 1.6$. The other parameters are the same as those in Fig. 2. Here x and y are in units of d_0 .

IV. STRUCTURE OF TWO-COMPONENT BECS WITH RESPECTIVE VAVSS WITH UNEQUAL WINDING NUMBERS OF VORTEX AND ANTIVORTEX

In Fig. 4, we present the typical structures of two-component BECs with respective VAVSS with $l_{jk} = 1$ and $l_{jp} = 2$ ($j = 1, 2$). Depending on the intra- and interspecies coupling strengths, the system shows different structures such as fully separated phases, inlaid separated phases, and partially mixed phases, which is similar to the case of $l_{jk} = l_{jp} = 1$ to some degrees. The density profile of each species in a fully mixed phase is similar to Fig. 4(e2) or Fig. 4(f1). Here an interesting characteristic is that the density profiles, except those of the inner species in partially mixed phases and the two species in a fully mixed phase, generally form closed (highly modulated petal-like) structures. The corresponding phase profiles are given in Fig. 5, where the value of the phase varies continuously from $-\pi$ to π , and the end point of the boundary between a π phase line and a $-\pi$ phase line represents a phase defect (anticlockwise rotation denotes a vortex while clockwise rotation denotes an antivortex).

For the cases of fully separated phases, we can see that there is a visible density hole in the density profile of the interior component [Figs. 4(a2) and 4(d1)] and a phase defect at the center of the corresponding phase profile [Figs. 5(a2) and 5(d1)]. The visible density hole is referred to as a visible vortex (anticlockwise rotation) [37] because the topological defect is visible in the *in situ* density profile and it contributes to the angular momentum and the energy of the system. At the same time, there are three phase singularities that locate

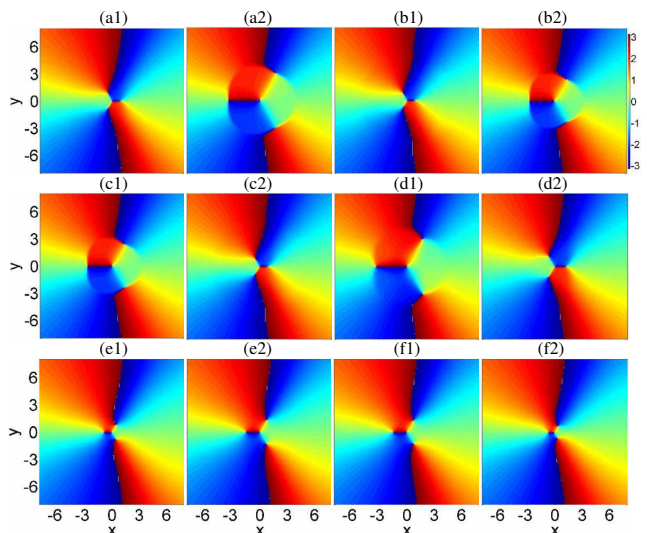


FIG. 5: (color online) Phase distributions corresponding to those of the density profiles of Fig. 4. The value of the phase varies continuously from $-\pi$ to π . The dark color area indicates the lower phase. Here x and y are in units of d_0 .

on the outskirts of the interior component and form a triangular lattice. Since these phase defects are invisible in the *in situ* density profile and contribute to neither the angular momentum nor the energy of the system, they are known as ghost vortices (exactly speaking, they are ghost antivortices because of their clockwise rotation) [37–39]. Of particular interest is the large density hole in the outer component [Figs. 4(a1) and 4(d2)]. From its phase distribution [Figs. 5(a1) and 5(d2)], we can see there are four phase defects in the region of density hole. The central phase defect is a vortex (anticlockwise rotation) and the peripheral three phase defects are antivortices (clockwise rotation) constituting a triangular lattice. The four topological defects are referred to as hidden vortices [37, 39, 40] because they carry significant angular momentum, though they are invisible in the *in situ* density distribution. Only after including the hidden vortices can the well-known Feynman rule [37, 43] be satisfied. The above analysis is also applicable to the cases of other states such as the inlaid separated-phase states and the mixed-phase states. For instance, for the partially mixed phases [Figs. 4(e), 4(f), 5(e), and 5(f)], there are four visible vortices in the density profile of each component in which one is a vortex lying on the trap center and the other are three antivortices locating on the periphery in a shape of triangular lattice.

In general, the phase defects distribute regularly. The trap center is always occupied by a vortex in both species 1 and species 2. For the partially mixed phases and the fully mixed phase, the outer antivortices in both components arrange in a triangular lattice at the almost same azimuth despite of different radiuses [Figs. 5(e1)-5(f2)]. For the separated phases, the outer three antivortices in species 1 and those in species 2 arrange successively

along the azimuth direction due to the strong intra- and interspecies repulsions as shown in Figs. 5(a1)-5(d2).

As for the other cases of $l_{1k} = l_{2k} \neq l_{1p} = l_{2p}$, our simulation shows that there exist similar phase structures. To understand the formation mechanism of the above phase structures, we consider a single-component BEC with a VAVSS with arbitrary unequal winding numbers $l_k \neq l_p$. As a general rule, we find that the steady state has $N = l_k + l_p$ peaks and $N + 1$ singularities in the phase distribution. When $l_k > l_p$, there are N singularities with unit positive topological charge on the periphery and l_p singularities with unit negative charge at the center, so that the total topological charge is $s = N - l_p = l_k$. When $l_k < l_p$, there are N singularities with unit negative charge on the periphery and l_k singularities with unit positive charge at the center, so that the total topological charge is $s = N - l_k = l_p$. For the case of $l_k = l_p$ and $\alpha^2 = \beta^2 = 1/2$, there is no phase singularity in the phase distribution due to the zero velocity field [28]. If $l_k = l_p$ and $\alpha^2 > \beta^2$ (or $\alpha^2 < \beta^2$), there would be l_k single-quantum vortices (or antivortices) at the trap center as a result of the larger vortex (antivortex) ratio α (β).

For a nonzero-temperature BEC in the presence of thermal atoms, a vortex state is generally unstable due to the incoherent interactions between the BEC and the thermal atoms [41]. For a zero-temperature BEC, a singly quantized vortex with repulsive interparticle interaction is stable while the stability of a multiply quantized vortex is determined by the property and strength of the interaction [42, 43]. Here an interesting question is what state a VAVSS with $l_k = 1$, $l_p = 2$, and $\alpha^2 = \beta^2 = 1/2$ will develop into. Counterintuitively, we find that the actual state is a vortex-antivortex cluster state consisting of a singly quantized vortex and three singly quantized antivortices. The density profile and the corresponding phase profile are similar to Fig. 4(e2) and Fig. 5(e2), respectively. The underlying physics is that in the presence of a single-quantum vortex the two-quantum antivortex only decays into three instead of two singly quantized antivortices because the triangular lattice [43, 44] has the lowest energy and is the most stable. It is well known that the angular momentum of a single vortex depends on its winding number while the average angular momentum per atom of a condensate is determined by not only the winding number but also the position of the vortex in the condensate. Combining with the conservation requirement of the average angular momentum per atom, then the vortex and the three antivortices rearrange themselves to a stable spacial structure with the lowest energy in which the vortex locates on the trap center and the three antivortices distribute on the outskirts by means of a triangular lattice form. The similar analysis can be generalized to the other cases. In Ref. [42], it is pointed out that a doubly quantized vortex may be stable in a BEC for certain regions of the interparticle interaction strength. In the present system, we do not observe similar doubly quantized antivortex in the equi-

librium structures (Fig. 4 and Fig. 5) even we change the values of the intra- and interspecies interaction strengths in a large scope. The dynamic processes and details of how the VAVSS decay into the vortex-antivortex cluster states require further investigation. Incidentally, when $l_{1k} = l_{1p} \neq l_{2k} = l_{2p}$ our simulation shows that the equilibrium density profiles may suffer from distortion even deletion of petals especially for those in a separated phase due to the symmetry breaking of two group winding numbers and the intra- and interspecies repulsions, which implies that the phase structures in this case will become quite complex. Further work would be necessary in order to understand the more complex structures in this case.

The petal structure of a VAVSS termed initially in Ref. [24] remind us of an azimuthon which is proposed lately in nonlinear optics [45] and extended recently to BECs [46]. We show that there exist evident difference and certain relation between the VAVSS and the azimuthon. The difference is that our theoretical model and the relevant studies [24–29] including the original literature [24] on the VAVSS work in the laboratory frame while the investigations concerning the azimuthon work in the rotation frame [45, 46]. Consequently, for the latter case there is an additional term with respect to angular velocity in the stationary equation of system [46]. The relation is that the azimuthon is a special example of the VAVSS in view of their solution expressions. For the same winding numbers of vortex and antivortex, the wave function of the VAVSS is given by $\varphi(r, \theta) \sim \alpha e^{i l \theta} + \beta e^{i \delta} e^{-i l \theta}$ [see also Eq. (5) in [28]]. If we take the relative phase $\delta = 0$ and introduce a parameter $p = (\alpha - \beta)/(\alpha + \beta)$, we can rewrite the wave function as $\varphi(r, \theta) \sim \cos(l\theta) + ip \sin(l\theta)$. Here the coefficient $\alpha + \beta$ has been absorbed in the normalization constant of the wave function, and the parameter p should satisfy the two conditions of $0 \leq |p| \leq 1$ and $\alpha^2 + \beta^2 = 1$. In this context, the azimuthon expressed by $\Phi \sim \cos(l\theta) + ip \sin(l\theta)$ in Refs. [45, 46] is indeed a particular case of the VAVSS. Obviously, a VAVSS is not equivalent to an azimuthon when $\delta \neq 0$. The similar analysis is also applicable to the cases of different winding numbers of vortex and antivortex.

V. CONCLUSION

We have numerically studied the exact 2D steady structures of two-component BECs with respective VAVSS. Depending on the winding numbers of vortex and antivortex and the intra- and intercomponent interactions, the system shows rich phase configurations such as fully separated phases, inlaid separated phases, asymmetric separated phase, and partially mixed phases with (deformed) petal-like component density distributions. For given parameters, we display a phase diagram of two-components with respective VAVSS with $l_{1k} = l_{1p} = 1$ and $l_{2k} = l_{2p} = 1$. We show that the kinetic energy plays a key role in determining the struc-

ture of the two-component BECs with respective VAVSS, where the conventional phase separation criterion is inapplicable and the TF approximation may fail due to the VAVSS, especially for the cases of VAVSS with large winding numbers. In addition, the conventional criterion for phase separation and the TF approximation can not discriminate different separated phases. According to the nonlinear stability analysis, the typical structures of the system are long-lived, which allows to be detected and tested in current experiments. The similar phase structures also exist in the two-component BECs with respective VAVSS with unequal winding numbers of vortex and antivortex. In this case, the density profile of each species forms a closed (highly modulated petal-like) structure except the fully mixed phase and the inner species in a partially mixed phase. In particular, an interesting vortex-antivortex cluster state occurs in each component in any of the possible phase structures, where the vortices and

antivortices appear in the form of visible vortex, or hidden vortex, or ghost vortex. Furthermore, a general relation between the vortex-antivortex cluster states and the winding numbers of vortex and antivortex is revealed and analyzed. Finally, we show that the azimuthon proposed recently in nonlinear optics and in BECs is a special example of VAVSS in terms of their solution expressions.

Acknowledgments

L.W. thanks Chuanwei Zhang, Biao Wu and Yongping Zhang for helpful discussion. This work was supported by the NSFC under Grants No. 11047033 and No. 10847143, the International Cooperation Program by Shandong Provincial Education Department, and the NSF of Shandong Province under Grant No. Q2007A01.

-
- [1] C. J. Pethick and H. Smith, *Bose-Einstein Condensation in Dilute Gases*, 2nd edn (Cambridge University Press, Cambridge, 2008).
- [2] L. Pitaevskii and S. Stringari, *Bose-Einstein Condensation* (Oxford University Press, Oxford, 2003).
- [3] T.-L. Ho and V. B. Shenoy, Phys. Rev. Lett. **77**, 3276 (1996).
- [4] H. Pu and N. P. Bigelow, Phys. Rev. Lett. **80**, 1130 (1998).
- [5] M. Trippenbach, K. Goral, K. Rzazewski, B. Malomed, and Y. B. Band, J. Phys. B **33**, 4017 (2000).
- [6] S. K. Adhikari, Phys. Rev. A **63**, 043611 (2001).
- [7] F. Riboli and M. Modugno, Phys. Rev. A **65**, 063614 (2002).
- [8] R. Navarro, R. Carretero-González, and P. G. Kevrekidis, Phys. Rev. A **80**, 023613 (2009).
- [9] G. Catelani and E. A. Yuzbashyan, Phys. Rev. A **81**, 033629 (2010).
- [10] G. Gligoric, A. Maluckov, M. Stepic, L. Hadzievski, and B. A. Malomed, Phys. Rev. A **82**, 033624 (2010).
- [11] L. Wen, W. M. Liu, Y. Cai, J. M. Zhang, and J. Hu, Phys. Rev. A **85**, 043602 (2012).
- [12] P. Kuopanportti, J. A. M. Huhtamäki, and M. Möttönen, Phys. Rev. A **85**, 043613 (2012).
- [13] S. B. Papp, J. M. Pino, and C. E. Wieman, Phys. Rev. Lett. **101**, 040402 (2008).
- [14] D. J. McCarron, H. W. Cho, D. L. Jenkin, M. P. Köppinger, and S. L. Cornish, Phys. Rev. A **84**, 011603 (2011).
- [15] C. Lee, Phys. Rev. Lett. **102**, 070401 (2009).
- [16] H. Takeuchi, S. Ishino, and M. Tsubota, Phys. Rev. Lett. **105**, 205301 (2010).
- [17] J. Sabbatini, W. H. Zurek, and M. J. Davis, Phys. Rev. Lett. **107**, 230402 (2011).
- [18] K. J. H. Law, P. G. Kevrekidis, and L. S. Tuckerman, Phys. Rev. Lett. **105**, 160405 (2010).
- [19] T. Kawakami, T. Mizushima, M. Nitta, and K. Machida, Phys. Rev. Lett. **109**, 015301 (2012).
- [20] A. Micheli, D. Jaksch, J. I. Cirac, and P. Zoller, Phys. Rev. A **67**, 013607 (2003).
- [21] Y. Zhang, L. Mao, and C. Zhang, Phys. Rev. Lett. **108**, 035302 (2012).
- [22] H. Takeuchi, N. Suzuki, K. Kasamatsu, H. Saito, and M. Tsubota, Phys. Rev. B **81**, 094517 (2010).
- [23] K. Sasaki, N. Suzuki, D. Akamatsu, and H. Saito, Phys. Rev. A **80**, 063611 (2009).
- [24] K. T. Kapale and J. P. Dowling, Phys. Rev. Lett. **95**, 173601 (2005).
- [25] M. Liu, L. H. Wen, H. W. Xiong, and M. S. Zhan, Phys. Rev. A **73**, 063620 (2006).
- [26] T. P. Simula, N. Nygaard, S. X. Hu, L. A. Collins, B. I. Schneider, and K. Molmer, Phys. Rev. A **77**, 015401 (2008).
- [27] S. Thanvanthri, K. T. Kapale, and J. P. Dowling, Phys. Rev. A **77**, 053825 (2008).
- [28] L. H. Wen, J. S. Wang, J. Feng, and H. Q. Hu, J. Phys. B **41**, 135301 (2008).
- [29] L. H. Wen, Y. P. Zhang, and J. Feng, J. Phys. B **43**, 225302 (2010).
- [30] S. K. Adhikari and L. Salasnich, Phys. Rev. A **75**, 053603 (2007).
- [31] M. F. Andersen, C. Ryu, P. Cladé, V. Natarajan, A. Vaziri, K. Helmerson, and W. D. Phillips, Phys. Rev. Lett. **97**, 170406 (2006).
- [32] K. C. Wright, L. S. Leslie, and N. P. Bigelow, Phys. Rev. A **77**, 041601 (2008).
- [33] K. C. Wright, L. S. Leslie, A. Hansen, and N. P. Bigelow, Phys. Rev. Lett. **102**, 030405 (2009).
- [34] M. Scherer, B. Lücke, G. Gebreyesus, O. Topic, F. Deuretzbacher, W. Ertmer, L. Santos, J. J. Arlt, and C. Klempt, Phys. Rev. Lett. **105**, 135302 (2010).
- [35] D. W. Peaceman and H. H. Rachford Jr., J. Soc. Indust. Appl. Math. **3**, 28 (1955).
- [36] Y. Zhang and B. Wu, Phys. Rev. Lett. **102**, 093905 (2009).
- [37] L. H. Wen, H. W. Xiong, and B. Wu, Phys. Rev. A **82**, 053627 (2010).
- [38] M. Tsubota, K. Kasamatsu, and M. Ueda, Phys. Rev. A **65**, 023603 (2002).
- [39] L. H. Wen and X. B. Luo, Laser Phys. Lett. **9**, 618 (2012).

- [40] M. Brtko, A. Gammal, and B. A. Malomed, Phys. Rev. A **82**, 053610 (2010).
- [41] D. S. Rokhsar, Phys. Rev. Lett. **79**, 2164 (1997).
- [42] H. Pu, C. K. Law, J. H. Eberly, and N. P. Bigelow, Phys. Rev. A **59**, 1533 (1999).
- [43] A. L. Fetter, Rev. Mod. Phys. **81**, 647 (2009).
- [44] J. R. Abo-Shaeer, C. Raman, J. M. Vogels, and W. Ketterle, Science **292**, 476 (2001).
- [45] A. S. Desyatnikov, A. A. Sukhorukov, and Y. S. Kivshar, Phys. Rev. Lett. **95**, 203904 (2005).
- [46] V. M. Lashkin, Phys. Rev. A **77**, 025602 (2008).